Higher-energy triplet-pair states in polyenes and their role in intramolecular singlet fission

D. J. Valentine,[1,2,*] D. Manawadu,[1] and W. Barford[1,2,†]

[1]*Department of Chemistry, Physical and Theoretical Chemistry Laboratory, University of Oxford, Oxford, OX1 3QZ, United Kingdom*

[2]*Balliol College, University of Oxford, Oxford, OX1 3BJ, United Kingdom*

(Received 9 July 2020; revised 12 August 2020; accepted 14 August 2020; published 8 September 2020)

Probing extended polyene systems with energy in excess of the bright state ($1\,^1B_u^+/S_2$) band edge generates triplets via singlet fission. This process is not thought to involve the $2\,^1A_g^-/S_1$ state, suggesting that other states play a role. Using density matrix renormalization group (DMRG) calculations of the Pariser-Parr-Pople-Peierls Hamiltonian, we investigate candidate states that could be involved in singlet fission. We find that the relaxed $1\,^1B_u^-$ and $3\,^1A_g^-$ singlet states and $1\,^5A_g^-$ quintet state lie below the S_2 state. The $1\,^1B_u^-$, $3\,^1A_g^-$, and $1\,^5A_g^-$ states are all thought to have triplet-pair character, which is confirmed by our calculations of bond dimerization, spin-spin correlation, and wave function overlap with products of triplet states. We thus show that there is a family of singlet excitations (i.e., $2\,^1A_g^-$, $1\,^1B_u^-$, $3\,^1A_g^-$, ...), composed of both triplet-pair and electron-hole character, which are fundamentally the same excitation, but have different center-of-mass energies. The lowest energy member of this family, the $2\,^1A_g^-$ state, cannot undergo singlet fission. But higher-energy members (e.g., the $3\,^1A_g^-$) state, owing to their increased kinetic energy and reduced electron-lattice relaxation, can undergo singlet fission for certain chain lengths.

DOI: 10.1103/PhysRevB.102.125107

I. INTRODUCTION

Current commercially available solar cell technology is impeded by the Shockley-Queisser limit, which means that higher-energy photons are not efficiently utilized for electricity generation [1]. When a high-energy photon is absorbed, the energy greater than the device's band gap is lost as heat. There are a number of different ways to better utilize the solar spectrum, one such option is singlet fission.

Singlet fission is a process in which a singlet exciton generated by photoexcitation evolves into two separate triplets [2]. Many polyene systems have been shown to exhibit this phenomenon [3–13]. If the two separate triplets have energy greater than or equal to the band gap of a photovoltaic carrier material, they can each generate a free electron-hole pair in the carrier material [14].

Singlet fission is often assumed to involve three processes or steps. The first step is state interconversion from the initial photoexcited state to a singlet state with triplet-pair character. After state interconversion the triplet pair is coherent and correlated. In the next step, the triplets migrate away from one another; this process can be described as a loss of electronic interaction. During this step, which is spin allowed, the triplets retain their spin coherence forming a geminate triplet pair in an overall singlet state. The final step involves the loss of spin coherence and leads to two independent triplets (or a nongeminate triplet pair) [15]. This step is not spin allowed and is expected to be slower than the preceding steps. Marcus and Barford have recently investigated this step using a Heisenberg spin chain model. They show how spin-orbital coupling and dephasing from the environment determines this process [15].

Polyene systems are often modeled as having C_{2h} symmetry [16–24]. In this framework, the first excited singlet state S_1 has the same symmetry as the ground state $1\,^1A_g^-$, and is therefore optically inactive. The strongly optically absorbing singlet state is the $1\,^1B_u^+$ state. Although this is not generally the second excited singlet state in polyenes, it is typically labeled S_2. In polyenes some low-energy excited states have multiple triplet excitation character [23]. This is the case for the $2\,^1A_g^-$ state, which is sometimes considered as a bound pair of triplet excitations [16–23].

In polyene systems it remains unclear if singlet fission proceeds via the $2\,^1A_g^-$ state, a vibrationally hot variant of the $2\,^1A_g^-$ state, or a different state [5,6,10]. It is also unclear whether singlet fission in polyene type materials is an inter- or intramolecular process [6,25,26]. It has been observed that in long isolated chains no singlet fission occurs after photoexcitation *at* the band edge. Instead, the system relaxes nonradiatively via the $2\,^1A_g^-$ state. The S_2 to S_1 transition occurs via internal conversion between the two potential energy surfaces [27], taking place on a timescale of 100s of fs [5,6,10]. Upon excitation with energy in excess of the band edge, however, triplets are detected, with isolated triplet signatures appearing in transient absorption spectroscopy measurements [5,6]. The occurrence of these triplet signals is attributed to singlet fission. Experiments suggest that this mid-band excited singlet fission does not proceed via the $2\,^1A_g^-$ state. It is claimed that there are two relaxation pathways: one to the ground state (which proceeds via the $2\,^1A_g^-$ state) and a different singlet fission pathway with no $2\,^1A_g^-$ involvement [5,6], as illustrated in Fig. 1.

If singlet fission in polyenes does not involve the $2\,^1A_g^-$ state, but does require excess energy to overcome a barrier,

*darren.valentine@chem.ox.ac.uk
†william.barford@chem.ox.ac.uk

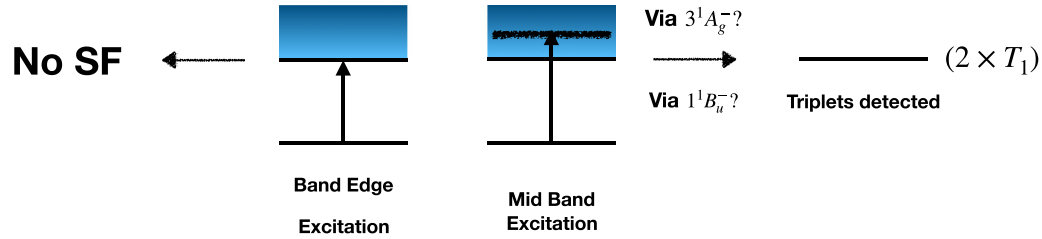

FIG. 1. Schematic of potential relaxation pathways from the bright state in polyenes.

it can be asked do any higher-energy states contribute? Upon vertical excitation it has been found that the $1\,^1B_u^-$ and $3\,^1A_g^-$ states exist above the $1\,^1B_u^+$, although as the chain length increases the $1B_u^-$ energy falls below the $1\,^1B_u^+$ [23,28]. It is also thought that the $1\,^1B_u^-$ and $3\,^1A_g^-$ states have triplet-pair character [23].

In addition to the singlet triplet-pair state, a quintet triplet-pair fission intermediate $^5(T_1T_1)$ has been observed in acene materials [29–31]. Spin mixing is possible between the $^1(T_1T_1)$ and $^5(T_1T_1)$ states [32], meaning the quintet could be involved in the singlet fission process or offer an alternative relaxation pathway for the excited molecule.

In this paper we present our calculations of the properties of the key excited states of polyenes, i.e., the $2\,^1A_g^-$, $1\,^1B_u^+$, $1\,^1B_u^-$, and $3\,^1A_g^-$ singlet states, the $1\,^5A_g^-$ quintet state, and the $1\,^3B_u^-$ triplet state. We use the Pariser-Parr-Pople-Peierls (or extended Hubbard-Peierls) model to describe interacting π electrons coupled to the nuclei, which is solved using the density matrix renormalization group (DMRG) method. We investigate the relaxed geometries of these states within a soliton framework. Excitations in polyene systems contain spin-density wave, bond-order excitations, and charge density waves. The interplay between these contributions leads to a myriad of phenomena [17]. To gain insight into the nature of the higher-energy excited states, we characterize the states using the spin-spin correlation function, and triplet-pair and electron-hole projections. We also investigate the optical transitions from these key states.

As we explain in the Discussion, we postulate that the $3\,^1A_g^-$ state (or another member of the "$2A_g$ family") is the spin-correlated $^1(T\cdots T)$ state, sometimes referred to as the geminate triplet pair, observed in the singlet fission process in polyenes. We find that the energetic conditions for a candidate singlet fission state is only met in sufficiently long chains described by a model that contains both electron-electron and electron-nuclear interactions. Using our model parameters, we tentatively predict that singlet fission is only possible in single polyene chains comprising 20 or more carbon atoms.

The paper is organized as follows. In Sec. II we introduce the Pariser-Parr-Pople-Peierls model. In Sec. III we discuss the results of our vertical and relaxed energy calculations. Section IV describes the solitonic structure of the geometrically relaxed excited states. In Sec. V we analyze the spin-spin correlation of these states. In Sec. VI we also characterize the states via their electron-hole and spinon wave functions, and their overlap with products of triplet states. In Sec. VII we relate our work to experimental results via a calculation of the excited state absorption spectra. Finally, we discuss our results and conclude in Sec. VIII.

II. PARISER-PARR-POPLE-PEIERLS MODEL

We use the Pariser-Parr-Pople-Peierls (PPPP) model to treat the π electrons of the conjugated system. This model includes both long-range electronic interactions and electron-nuclear coupling. It is defined as [17]

$$H_{\mathrm{PPPP}} = H_{\mathrm{PPP}} + H_{\text{el-ph}} + H_{\mathrm{elastic}}, \tag{1}$$

where H_{PPP} is the Pariser-Parr-Pople (or extended Hubbard) Hamiltonian, defined by

$$H_{\mathrm{PPP}} = -2t_0 \sum_n \hat{T}_n + U \sum_n \left(N_{n\uparrow} - \frac{1}{2}\right)\left(N_{n\downarrow} - \frac{1}{2}\right) + \frac{1}{2}\sum_{n\neq m} V_{n,m}(N_n - 1)(N_m - 1). \tag{2}$$

Here $\hat{T}_n = \frac{1}{2}\sum_\sigma (c^\dagger_{n,\sigma}c_{n+1,\sigma} + c^\dagger_{n+1,\sigma}c_{n,\sigma})$ is the bond order operator, t_0 is the hopping integral for a uniform, undistorted chain, U is the Coulombic interaction of two electrons in the same orbital, and V_{nm} is the long-range Coulombic repulsion. We use the Ohno potential given by $V_{nm} = U/[1 + (U\epsilon_r r_{nm}/14.397)^2]^{1/2}$, with bond lengths r_{nm} in Å.

$H_{\text{el-ph}}$ is the electron-phonon coupling, given by

$$H_{\text{el-ph}} = 2\alpha \sum_n (u_{n+1} - u_n)\hat{T}_n - 2\alpha W \sum_n (u_{n+1} - u_n) \times (N_{n+1} - 1)(N_n - 1), \tag{3}$$

where α is the electron-nuclear coupling parameter and u_n is the displacement of nucleus n from its undistorted position. Through this term changes in bond length cause changes in the hopping integrals and the Coulomb interactions. Due to the rapid decay of the density-density correlator, $(N_n - 1)(N_m - 1)$ with distance, only changes in the Coulomb potential to first order are considered. Therefore, $W = U\gamma r_0/(1 + \gamma r_0^2)^{3/2}$, where $\gamma = (U\epsilon_r/14.397)^2$ and r_0 is the undistorted average bond length in Å.

The elastic energy of the nuclei contributes through H_{ph}, defined as

$$H_{\mathrm{ph}} = \frac{\alpha^2}{\pi t_0 \lambda}\sum_n (u_{n+1} - u_n)^2 + \Gamma \sum_n (u_{n+1} - u_n), \tag{4}$$

where $\lambda = 2\alpha^2/\pi K t$ is the dimensionless electron-nuclear coupling parameter and K is the nuclear spring constant. Γ is a Lagrange multiplier which ensures a constant chain length.

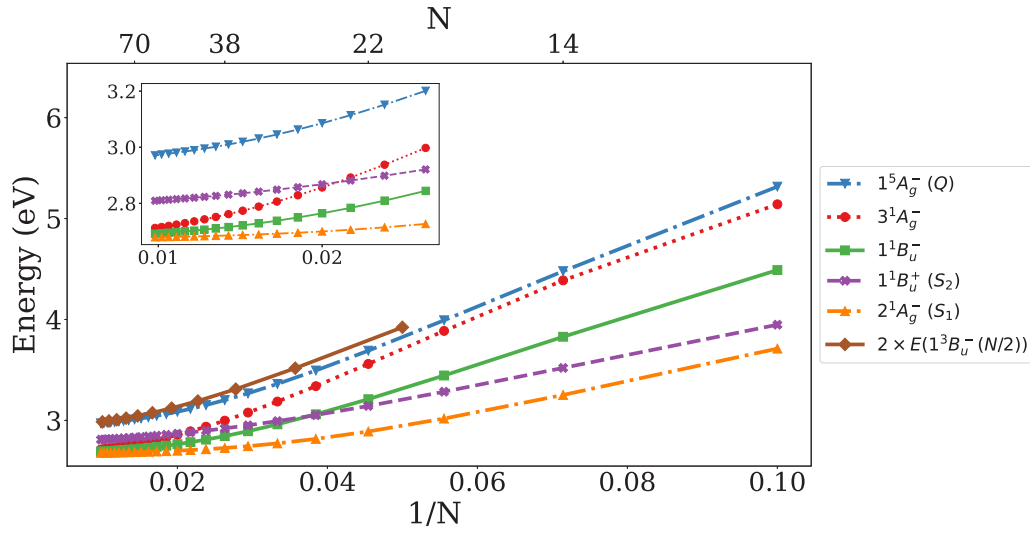

FIG. 2. Vertical excitation energy of low-lying singlet and quintet states. Also shown is twice the vertical excitation energy of the triplet for chain lengths $N/2$. N is the number of C atoms. The inset shows the energies in the asymptotic limit.

The requirement that the force per bond vanishes at equilibrium gives a self-consistent equation for the bond distortion via the Hellmann-Feynman theorem, namely

$$(u_{n+1} - u_n) = \frac{\pi t \lambda}{\alpha}(\Gamma - \langle \hat{T}_n \rangle + W \langle \hat{D}_n \rangle), \tag{5}$$

where $\hat{D}_n = (N_n - 1)(N_{n+1} - 1)$ is the nearest neighbor density-density correlator. We follow a parametrization of the PPP Hamiltonian by Mazumdar and Chandross for *screened* polyacetylene [33], namely $U = 8$ eV, $\epsilon_r = 2$, and $t_0 = 2.4$ eV. We use the electron-nuclear coupling constants of Barford and co-workers, namely, $\lambda = 0.115$ and $\alpha = 0.4593$ eV Å^{-1} [18].

For a fixed set of nuclear coordinates we solve the PPPP model using the DMRG method [18,34,35]. DMRG is a highly accurate and robust computational method for gapped, one-dimensional quantum lattice models. Being variational, its accuracy is systematically improvable by increasing the Hilbert space size. Extensive convergence tests on the application of the DMRG method to the excited states of the PPPP model have previously been published [16,36–38]. For the current calculations we typically retained over 400 states per block. In addition, when investigating possible energy crossovers between pairs of excited states, we compute these states using the same reduced density matrix (i.e., in the same truncated Hilbert space). The relaxed geometries are found via an iterative application of Eq. (5).

III. VERTICAL AND RELAXED ENERGIES

The calculated vertical excitation energies (using the relaxed ground state geometry) for the lowest energy singlets are shown in Fig. 2. For short chains we see the usual energetic ordering of $2\,^1A_g^- < 1\,^1B_u^+ < 1\,^1B_u^- < 3\,^1A_g^-$ [23,39]. For chain lengths greater than 26 sites the vertical $1\,^1B_u^-$ energy becomes lower than the $1\,^1B_u^+$ energy, while at chain lengths greater than 46 sites the $3\,^1A_g^-$ vertical energy falls below the $1\,^1B_u^+$ energy.

The $1\,^5A_g^-$ quintet state, however, remains above the bright state at all chain lengths. Its energy converges to twice the triplet energy evaluated at half the chain length, implying that it corresponds to an unbound triplet pair. This assumption will be confirmed by an analysis of the bond dimerization and spin-spin correlation in the following sections [40].

The inset of Fig. 2 shows that the vertical energies of the $2\,^1A_g^-$, $1\,^1B_u^-$, and $3\,^1A_g^-$ states converge to the same value in the asymptotic limit, being ∼0.3 eV lower than the vertical quintet state. This result indicates that these vertical singlet states are different pseudomomentum members of the same family of excitations, as described in more detail in Sec. VI. They have different energies because of their different center-of-mass kinetic energies, which vanishes in the long-chain limit.

Turning now to the relaxed energies, as shown in Fig. 3 we find that the relaxed $2\,^1A_g^-$ state is always lower in energy than the relaxed $1\,^1B_u^+$ state. For chain lengths greater than 10 and 20 sites the $1\,^1B_u^-$ and $3\,^1A_g^-$ states, respectively, also fall below the $1\,^1B_u^+$ state. The quintet state undergoes a considerable geometry relaxation compared to the $1\,^1B_u^+$ state and its energy falls below the bright state for $N > 16$.

Comparing the vertical and relaxed energies, we find that between 10 and 26 sites the vertical $1\,^1B_u^-$ state lies above the vertical $1\,^1B_u^+$ state, but the relaxed $1\,^1B_u^-$ state is below the relaxed $1\,^1B_u^+$ state; and similarly for the $3\,^1A_g^-$ state between 20- and 46-site chains. Thus our calculations suggest that there might exist internal conversion pathways to these states from the optically excited $1\,^1B_u^+$ state. In addition, if spin mixing is allowed relaxation pathways could also involve the $1\,^5A_g^-$ quintet state. Based on the experimental observations that certain relaxation pathways becoming available only for mid-band or higher excitation [5,10], these pathways are likely to have a barrier.

The $2A_g^-$ state is found to be a bound state compared to two free (relaxed) triplets. While endothermic singlet fission is possible [41,42], this state is unlikely to be involved in singlet fission and instead offers an alternative relaxation pathway, as

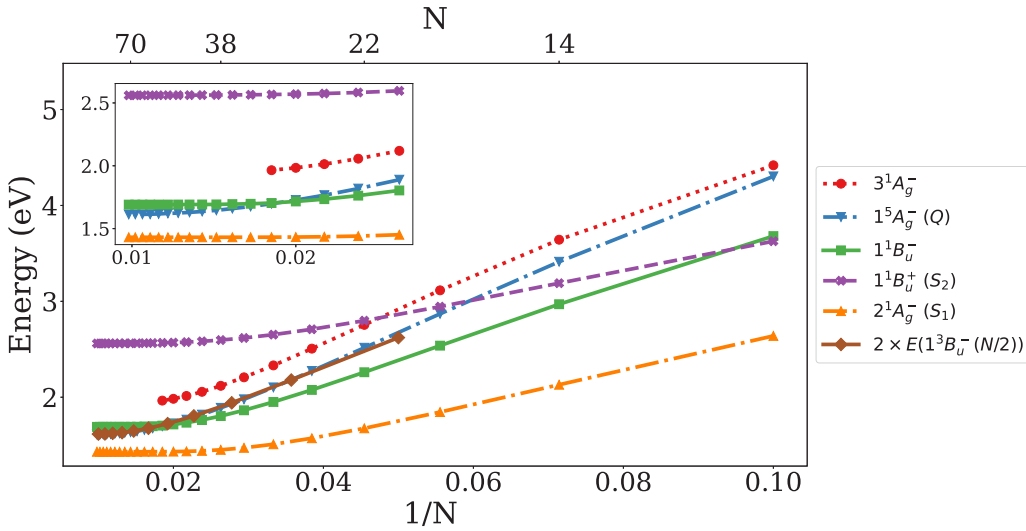

FIG. 3. Relaxed excitation energy of low-lying singlet and quintet states. Also shown is twice the relaxed excitation energy of the triplet for chain lengths $N/2$. N is the number of C atoms. The inset shows the energies in the asymptotic limit.

has been observed experimentally [5,6]. Similarly, for realistic chain lengths (i.e., up to approximately 50 C atoms) the relaxed $1\,^1B_u^-$ energy lies below the relaxed energy of two free triplets, while the relaxed $3\,^1A_g^-$ energy lies above them for all chain lengths. As for the vertical calculation, for the relaxed states we find that $E(1\,^5A_g^-) \approx 2 \times E(1\,^3B_u^-[N/2])$.

We note that the relaxation energies increase as $3\,^1A_g^- < 1\,^1B_u^- < 2\,^1A_g^-$. (For example, at 50 C atoms the relaxation energies of the $3\,^1A_g^-$, $1\,^1B_u^-$, and $2\,^1A_g^-$ states are 0.87, 1.04, and 1.27 eV, respectively, while the relaxation energy of the $1\,^5A_g^-$ state is 1.36 eV). We do not have clear explanation for this trend, but speculate that it is associated with the smaller triplet-pair components of the higher-energy momentum states at shorter chain lengths, as shown in Table I.

Consequently, unlike the vertical energies, the relaxed energies of the $2\,^1A_g^-$, $1\,^1B_u^-$, and $3\,^1A_g^-$ states do not converge to the same value in the asymptotic limit, and indeed they saturate for $N \gtrsim 50$. This energy saturation occurs because of self-localization of the solitons, which is a consequence of treating the nuclei as classical variables and can be corrected by using a model of fully quantized nuclei [17,36] In practice, however, in realistic systems disorder will also act to localise excited states [43].

TABLE I. Table of the square of overlaps $|\langle T_l \otimes T_r \,|\, \Psi\rangle|^2$ for the vertical $2\,^1A_g^-$, $1\,^1B_u^-$, and $3\,^1A_g^-$ states. T_r and T_l are calculated for a 6-site chain (the superscript indicates the S_z eigenvalue of the state, T_1 and T_2 corresponds to the $1\,^3B_u^-$ and $1\,^3A_g^-$ triplets, respectively), while the state Ψ is calculated for a 12-site chain.

		$\lvert\langle T_l \otimes T_r \,\rvert\, \Psi\rangle\rvert^2_v$		
T_l	T_r	$2\,^1A_g^-$	$3\,^1A_g^-$	$1\,^1B_u^-$
T_1^0	T_1^0	0.134	0.020	–
T_1^{+1}	T_1^{-1}	0.134	0.020	–
T_1^{-1}	T_1^{+1}	0.134	0.020	–
T_1^0	T_2^0	0.010	0.012	0.022
T_2^0	T_1^0	0.010	0.012	0.022
T_1^{+1}	T_2^{-1}	0.010	0.012	0.022
T_2^{-1}	T_1^{+1}	0.010	0.012	0.022
T_2^{+1}	T_1^{-1}	0.010	0.012	0.022
T_1^{-1}	T_2^{+1}	0.010	0.012	0.022
T_2^0	T_2^0	–	0.015	–
T_2^{+1}	T_2^{-1}	–	0.015	–
T_2^{-1}	T_2^{+1}	–	0.015	–
Total		0.462	0.177	0.132

IV. SOLITON STRUCTURES

In the even N polyene ground state, nuclei are dimerized along the chain, with a repeated short-long-short bond arrangement. Electronically excited states lower their total energy by distorting from the ground state geometry. In some cases, the ground state bond alternations is reduced or reversed over sections of the chain. The change of dimerization is characterized by domain walls called solitons [17,18,44–47]. In neutral chains with an even number of sites, each soliton (S) is associated with an antisoliton ($\bar{S}$).

Solitons in linear conjugated systems are of two types: radical or ionic. For a radical soliton associated with covalent states the nuclei distortion is centered around a radical unpaired spin (or a spinon); the soliton has a net spin but is neutral. For an ionic soliton, however, the distortion is associated with an unoccupied or doubly occupied site, so has $S^z = 0$ but is charged [17,46].

To investigate the solitonic structure of the excited singlet and quintet states, we calculate the staggered, normalized bond dimerization δ_n of their relaxed geometries, defined as

$$\delta_n = (-1)^n \frac{(t_n - \bar{t})}{\bar{t}}, \tag{6}$$

with $t_n = t_0 + \alpha(u_{n+1} - u_n)$ and $\bar{t}$ being the average of t_n. For the ground state $\delta_n \approx 0.085$, across the chain with the bond dimerization being slightly larger at the ends of the chain.

The lowest lying triplet state $1\,^3B_u^-$ is a two-soliton state (i.e., $S\bar{S}$) with each soliton being associated with a radical spin, residing towards the ends of the chain. On the other hand, the $2\,^1A_g^-$, $1\,^1B_u^-$, and $1\,^5A_g^-$ states are four-soliton states.

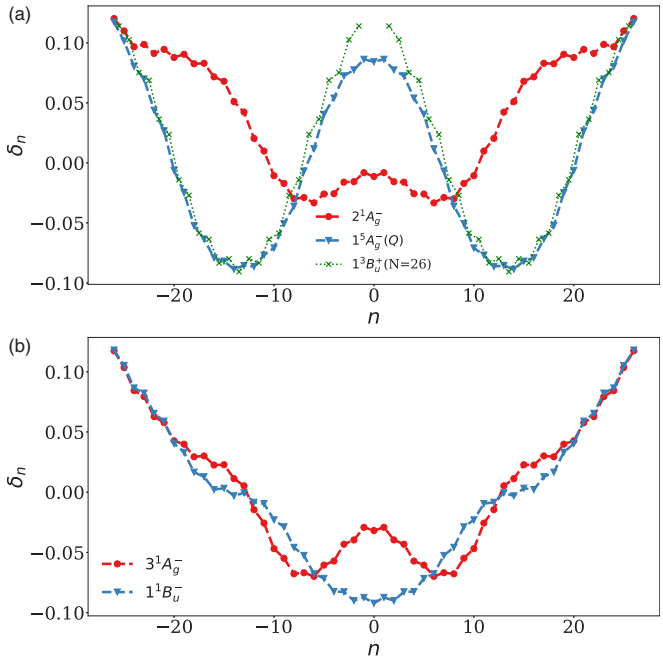

FIG. 4. The staggered bond dimerization δ_n for a chain of 54 sites, of the (a) $2\,^1A_g^-$, $1\,^5A_g^-$, and $1\,^3B_u^-$ (for $N = 26$) states and (b) $1\,^1B_u^-$ and $3\,^1A_g^-$ states.

Figure 4(a) presents the staggered bond dimerization for the $2\,^1A_g^-$ and $1\,^5A_g^-$ states, implying that the soliton arrangement is $S\bar{S}S\bar{S}$. The $1\,^5A_g^-$ bond dimerization strongly resembles that of two triplets residing on either half of the chain, suggesting that this state consists of two spatially separated triplets. The bond dimerization of the $2\,^1A_g^-$ state is well known [18,23,24,44,45,47]: the solitons are more bound, indicating that the $2\,^1A_g^-$ state is a bound triplet pair. These observations are quantified by fitting the bond dimerization of the $2\,^1A_g^-$ and $1\,^5A_g^-$ states by [47]

$$\delta_n = \delta_0\Bigg[1 + \tanh\left(\frac{2n_0a}{\xi}\right)\Bigg\{\tanh\left(\frac{2(n-n_d-n_0)a}{\xi}\right) - \tanh\left(\frac{2(n-n_d+n_0)a}{\xi}\right) + \tanh\left(\frac{2(n+n_d-n_0)a}{\xi}\right) - \tanh\left(\frac{2(n+n_d+n_0)a}{\xi}\right)\Bigg\}\Bigg], \tag{7}$$

where ξ is the domain wall width, $2n_0$ is the separation of the soliton and antisoliton within a $S\bar{S}$ pair on either side of the chain, while $2n_d$ is the separation of the pairs.

The bond dimerization of the $1\,^1B_u^-$ state, shown in Fig. 4(b), can be explained by the soliton arrangement of $SS\bar{S}\bar{S}$. Its bond dimerization fits the equation

$$\delta_n = \delta_0\Bigg[1 + \frac{1}{2}\tanh\left(\frac{2n_0a}{\xi}\right)\Bigg\{\tanh\left(\frac{2(n-n_d-n_0)a}{\xi}\right) + \tanh\left(\frac{2(n-n_d+n_0)a}{\xi}\right) - \tanh\left(\frac{2(n+n_d-n_0)a}{\xi}\right) - \tanh\left(\frac{2(n+n_d+n_0)a}{\xi}\right)\Bigg\}\Bigg], \tag{8}$$

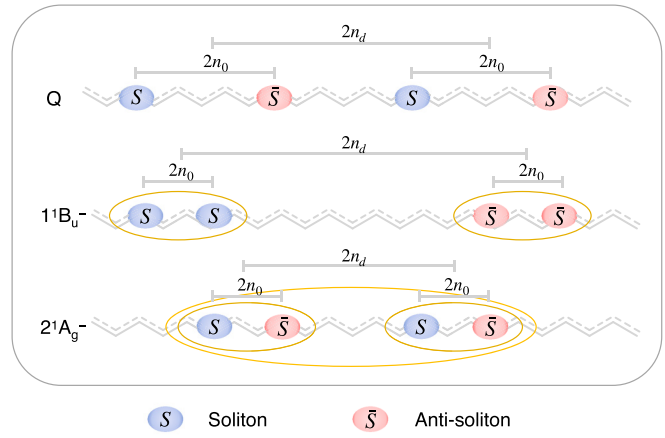

FIG. 5. The solitonic arrangement of the $1\,^5A_g^-$ (Q), $1\,^1B_u^-$, and $2\,^1A_g^-$ states, and also illustrating the definition of n_0 and n_d.

where $2n_0$ is the separation of the soliton and soliton within a SS pair (and likewise of the antisoliton and antisoliton within a $\bar{S}\bar{S}$ pair), while $2n_d$ is the separation of these pairs. The solitonic arrangement, and the definition of n_0 and n_d are illustrated in Fig. 5.

We are unable to fit the $3\,^1A_g^-$ state bond dimerization to either Eqs. (7) or (8). As we will see in Sec. VI A, there are many different triplet-pair contributions to the $3\,^1A_g^-$ state causing a complicated bond dimerization.

The fitted parameters n_0, n_d, and ξ, for three four-soliton states are plotted in Fig. 6 against inverse chain length. In Fig. 6(a) we see that the coherence length ξ converges with chain length for all states.

The rapid convergence of n_0 with chain length for the $2\,^1A_g^-$ state, shown in Fig. 6(b), implies that the solitons within a $S\bar{S}$ pair are more strongly bound compared to other states. For the $1\,^5A_g^-$ state, the change in n_0 with chain length N resembles that of the $1\,^3B_u^-$ state for a chain of half-length $N/2$, indicating that the $1\,^5A_g^-$ state has significant T_1-T_1 character with two tripletlike excitations occupying either side of the chain. n_0 converges as a function of N for the $1\,^1B_u^-$ state, implying that the solitons (antisolitons) within a SS ($\bar{S}\bar{S}$) pair are bound.

The distances between soliton pairs n_d are shown in Fig. 6(c). Again, for the $2\,^1A_g^-$ state there is rapid convergence in the separation of these pairs. In contrast, both the $1\,^5A_g^-$ and $1\,^1B_u^-$ states do not show convergence, with the pair separation increasing as the chain length increases. For the $1\,^5A_g^-$ state $n_d \approx N/4$, again indicating that the pairs are unbound. We also observe that for chains of more than ∼50 carbon atoms n_d increases more quickly for the $1\,^1B_u^-$ state than for the $1\,^5A_g^-$ state. As shown in the inset of Fig. 3, this deviation coincides with the relaxed energy of the $1\,^1B_u^-$ state being higher than the $1\,^5A_g^-$ state for $N \gtrsim 50$, implying that at large chain lengths the triplets in the relaxed $1\,^1B_u^-$ state are unbound with respect to pairs of relaxed triplets. The solitons (or spinons) in the $1\,^1B_u^-$ state are not "free," however, as n_0 converges with chain length. (We note that the triplets in the relaxed $3\,^1A_g^-$ state are unbound with respect to pairs of relaxed triplets for all chain lengths because, as we saw in Sec. III, the electron-

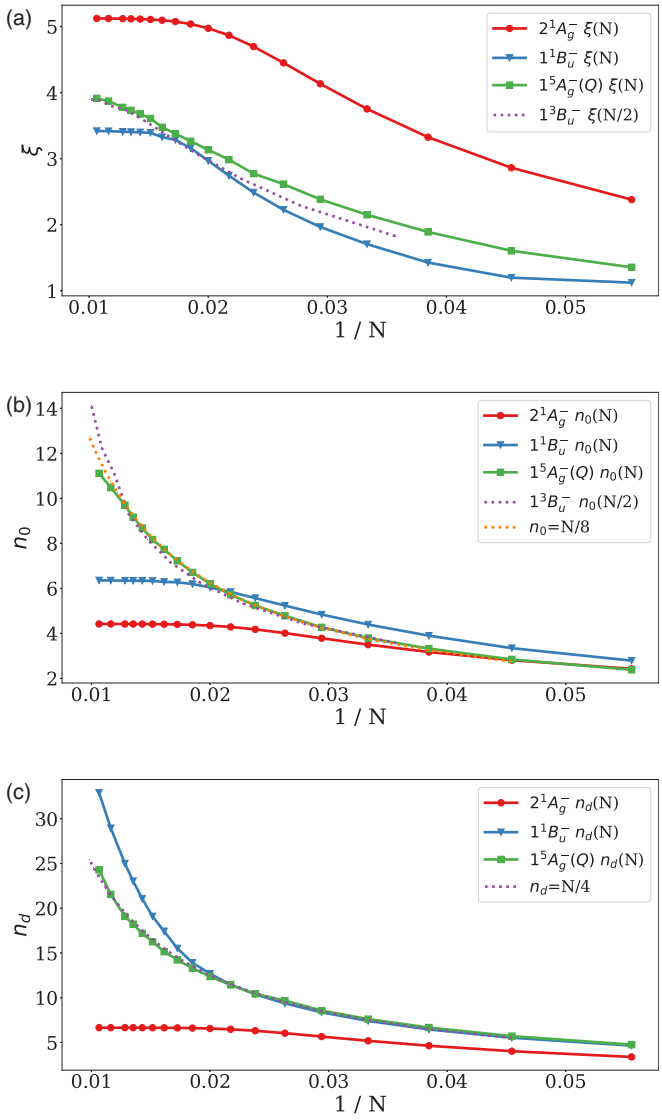

FIG. 6. The fitted parameters, (a) ξ_i, (b) n_0, and (c) n_d plotted against inverse chain length for the four-soliton states $2\,^1A_g^-$, $1\,^5A_g^-$, and $1\,^1B_u^-$. For comparison, in (a) the $1\,^3B_u^-$ n_0 for length $N/2$, in (b) the $1\,^3B_u^-$ coherence length ξ for length $N/2$ is plotted, and in (c) the curve $n_d = N/4$ is plotted.

lattice relaxation energy decreases with increasing kinetic energy, causing a crossover of the $3\,^1A_g^-$ and $1\,^5A_g^-$ energies).

V. SPIN-SPIN CORRELATION

In addition to the bond dimerization, further insight into the radical (spinon) character of the triplet-pair states is obtained via the spin-spin correlation function $S_{nm} = \langle S_n^z S_m^z \rangle$. A positive/negative spin-spin correlation value indicates a ferromagnetic/antiferromagnetic alignment between a pair of spins.

The spin-spin correlations for the relaxed $1\,^3B_u^-$ state are shown in Fig. 7(a). We see that the radical soliton/antisoliton of the triplet state localize towards the end of the chain and there is a long-range spin-spin correlation between them. The solitons are delocalized over a small region well described by the coherence length ξ.

Figure 7(e) shows the spin-spin correlation for the relaxed $1\,^5A_g^-$ state. We see three correlations between neighboring solitons and antisolitons, and three further long-range correlations. This correlation pattern is consistent with two unbound triplets, i.e., four solitons positioned along the chain as predicted from Eq. (7) and presented in Fig. 4(a). A schematic of the soliton interactions that lead to these six correlations is shown in Fig. 7(f).

Figure 7(b) shows S_{nm} for the $2\,^1A_g^-$ state. It is difficult to discern correlations between individual solitons, because the correlations overlap each other. However, along the antidiagonal $m = (N - n)$, long-range correlations between sites ≈ 10 and ≈ 40 can be seen. Overall, the spin-spin correlations of the $2\,^1A_g^-$ state further confirm its bound triplet-pair character. The triplets are bound in the middle of the chain, and individual solitons contributing to the triplets cannot be identified. S_{nm} for the relaxed $1\,^1B_u^-$ state shows correlations similar to $3\,^1A_g^-$, but with much more delocalized correlations along the antidiagonal.

VI. EXCITED STATE WAVE FUNCTIONS

The low-lying singlet dark states, i.e., $2\,^1A_g^-$, $1\,^1B_u^-$, and $3\,^1A_g^-$, have negative particle-hole symmetry and are sometimes characterized as being "covalent" or of predominately spin-density-wave (SDW) character [48]. In contrast, the optically allowed $1\,^1B_u^+$ state has positive particle-hole symmetry and is characterized as being "ionic" or of electron-hole character [49].

In practice, however, the "multiexcitonic" $2\,^1A_g^-$, $1\,^1B_u^-$, and $3\,^1A_g^-$ states have both covalent and ionic character. In addition, as we saw in Sec. III, the vertical energies of these states converge to the same value as $N \to \infty$ (see the inset of Fig. 2), suggesting that they are related. In this section we describe the multiexcitonic character of these states and explain how they are members of the same family of excitations. We first discuss the triplet-pair components of these states before describing their excitonic wave functions.

A. Triplet-triplet overlap

By comparing the excitation energy of the low-energy singlets of polyenes with the excitation energy of the individual triplets, it has been suggested that the triplet-pair combinations that contribute to each state are [23,27]

$$\begin{aligned} 2\,^1A_g^- &\equiv T_1 \otimes T_1, \\ 1\,^1B_u^- &\equiv T_1 \otimes T_2, \\ 3\,^1A_g^- &\equiv T_2 \otimes T_2, \end{aligned} \tag{9}$$

where $T_1 \equiv 1\,^3B_u^-$ and $T_2 \equiv 1\,^3A_g^-$.

To quantify the triplet-pair character of the $2\,^1A_g^-$, $3\,^1A_g^-$, and $1\,^1B_u^-$ singlet states we compute their overlap with triplet-pair direct product wave functions. We calculate the vertical excited state wave functions for a chain of 12 sites. Then, by calculating the triplet states for a chain of 6 sites and taking the direct product of different pairs of triplets, we can

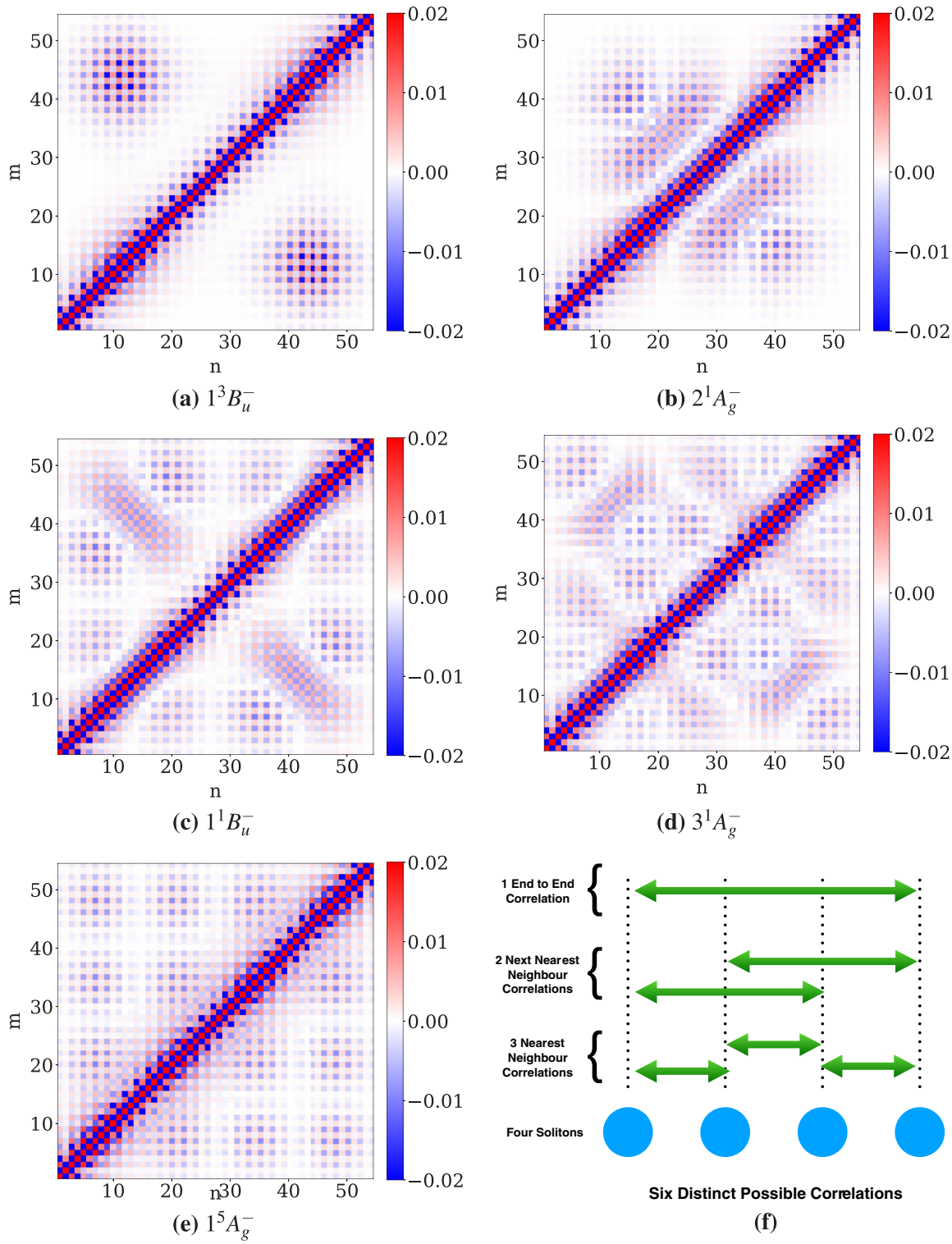

FIG. 7. The spin-spin correlations for the relaxed (a) $1\,^3B_u^-$, (b) $2\,^1A_g^-$, (c) $1\,^1B_u^-$, (d) $3\,^1A_g^-$, and (e) $1\,^5A_g^-$ states. (f) A schematic of the correlations from the four spin radicals (or spinons) of the $1\,^5A_g^-$ state. (Note that the values of S_{nm} for $n = m$ to $n = m \pm 4$ are larger than scale provided. The scale presented is used to emphasize the long-range correlations).

generate states that have triplets on either half of the chain. The square overlap of the triplet-pair wave functions with the $2\,^1A_g^-$, $3\,^1A_g^-$, and $1\,^1B_u^-$ states are presented in Table I.

The $2\,^1A_g^-$ state, while primarily consisting of $T_1 \otimes T_1$ components, also contains some $T_1 \otimes T_2$ character. The $1\,^1B_u^-$ state consists exclusively of $T_1 \otimes T_2$, as only these combinations are symmetry allowed. The $3\,^1A_g^-$ state, rather than primarily having $T_2 \otimes T_2$ character, has both $T_1 \otimes T_1$ and symmetry allowed combinations of T_1 and T_2 components in its wave function. Indeed, the sum of the $T_1 \otimes T_1$ and

$T_1 \otimes T_2$ components has a larger amplitude than the $T_2 \otimes T_2$ character. Since the $3\,^1A_g^-$ state has character from each of the triplet-pair combinations, the sum of these contributions lead to the complicated staggered bond dimerization and spin-spin correlation, discussed in Secs. IV and V.

B. Triplet-pair bound states

In the previous section we saw that higher-energy covalent states are composed of linear combinations of higher-energy triplet states. In this section we quantify how to construct bound triplet-pair states from free triplet-pair states. To do this it is convenient to assume translationally invariant systems. We also assume a dimerized antiferromagnetic ground state, from which bound triplet-pair excitations are predicted [50,51].

Suppose that $a_{k_1}^\dagger$ and $a_{k_2}^\dagger$ create triplet excitations (or more precisely, bound spinon-antispinon pairs [51]) with wave vectors k_1 and k_2. Then a free triplet-pair excitation is

$$|k_1, k_2\rangle = |K - k'/2, K + k'/2\rangle = a_{k_1}^\dagger a_{k_2}^\dagger |\mathrm{GS}\rangle\,, \tag{10}$$

where $2K = (k_1 + k_2)$ is a the center-of-mass wave vector, $k' = (k_1 - k_2)$ is the relative wave vector, and $|\mathrm{GS}\rangle$ represents the dimerized antiferromagnetic ground state.

A bound triplet-pair excitation is a linear combination of the kets $\{|k_1, k_2\rangle\}$, namely

$$|\Phi_n(K)\rangle = \sum_{k',K'} \Phi_n(k', K')\,|K' - k'/2, K' + k'/2\rangle\,, \tag{11}$$

where $\Phi_n(k', K')$ is the triplet-pair wave function in k space and n is the principal quantum number. K is a good quantum number for the bound state (although k' is not), hence

$$\Phi_n(k', K') = \psi_n(k')\delta(K' - K) \tag{12}$$

and thus

$$|\Phi_n(K)\rangle = \sum_{k'} \psi_n(k')\,|K - k'/2, K + k'/2\rangle\,. \tag{13}$$

Fourier transforming $\Phi_n(k', K')$ gives the real-space triplet-pair wave function

$$\tilde{\Phi}_{n,K}(r, R) = \tilde{\psi}_n(r)\tilde{\Psi}_K(R), \tag{14}$$

where the center-of-mass wave function is the Bloch state

$$\tilde{\Psi}_K(R) = \frac{1}{\sqrt{N}} \exp(iKR) \tag{15}$$

and R is the center-of-mass coordinate. $\tilde{\psi}_n(r)$ is the relative wave function with r being the T-T separation.

Equation (13) indicates that the bound triplet-pair state is constructed from a linear combination of free triplet-pair states with different k_1 and k_2, subject to a definite center-of-mass wave vector (and momentum). These states form a band, whose bandwidth is determined by their center-of-mass kinetic energy. A bound triplet pair is unstable to dissociation (or fission) if its kinetic energy is greater than the triplet-pair binding energy.

C. Exciton wave functions

We now describe the exciton wave functions of the low-energy states of linear polyenes, using a real-space representation. The excitation of an electron from the valence band to the conduction band in semiconductors creates a positively charged hole in the valence band. In conjugated polymers, the electrostatic interaction between the two create a bound electron-hole pair, termed an exciton. Assuming the "weak-coupling" limit, excitons in conjugated polymers are described by an effective H-atom model [17,52,53] or by a mapping from a single-CI calculation [54]. An excitation from the valence band to the conduction band can thus be characterized by an effective particle model [17]. In the real-space picture, an exciton is described by the center-of-mass coordinate of the exciton R and the relative coordinate r [17]. r is a measure of the size of the exciton. The electron-hole coordinate r is associated with the principal quantum number n [17,52,53], while the center-of-mass coordinate is associated with the center-of-mass quantum number j.

We denote an exciton basis state by $|R + r/2, R - r/2\rangle$. The exciton creation operator $S_{rR}^\dagger$ creates a hole in the valence-band orbitals at $(R - r/2)$ and an electron in the conduction-band orbitals at $(R + r/2)$, i.e.,

$$|R + r/2, R - r/2\rangle = S_{rR}^\dagger |\mathrm{GS}\rangle\,, \tag{16}$$

where $|\mathrm{GS}\rangle$ is the ground state in this basis.

To investigate the electron-hole nature of the excited states, we express an excited state $|\Phi\rangle$ as a linear combination of the real-space exciton basis $\{|R + r/2, R - r/2\}\rangle$:

$$|\Phi\rangle = \sum_{r,R} \Phi(r, R)\,|R + r/2, R - r/2\rangle\,. \tag{17}$$

$\Phi(r, R)$ is the exciton wave function and is given by the projection of the excited states on to the ground state

$$\Phi(r, R) = \langle \mathrm{GS}|S_{rR}|\Phi\rangle. \tag{18}$$

The calculated vertical exciton wave functions for the $1\,^1B_u^+$, $1\,^1A_g^+$, $2\,^1A_g^-$, $1\,^1B_u^-$, and $3\,^1A_g^-$ states of chain of $L = 102$ are illustrated in Fig. 8. The nodal patterns of $\Phi(r, R)$ indicate that the $1\,^1B_u^+$ and $1\,^1A_g^+$ states have components belonging to the $n = 1$ family of (even-parity) excitons with center-of-mass quantum numbers $j = 1$ and 2, respectively. This confirms the well-known result that the $1\,^1B_u^+$ state (or S_2) is the lowest energy member of the band of Frenkel excitons [17].

Similarly, the $2\,^1A_g^-$, $1\,^1B_u^-$, and $3\,^1A_g^-$ states have components belonging to the $n = 2$ family of (odd-parity) excitons with center-of-mass quantum numbers $j = 1$, 2, and 3, respectively. Thus, the single electron-hole components of the $2\,^1A_g^-$, $3\,^1A_g^-$, and $1\,^1B_u^-$ states belong to the same fundamental excitation. We note, however, that the electron-hole weights for these states are five times smaller than for the $1\,^1B_u^+$ and $1\,^1A_g^+$ states.

D. The $2A_g$ family

As we have shown, the $2\,^1A_g^-$, $1\,^1B_u^-$, and $3\,^1A_g^-$ states have both triplet-pair and electron-hole components. For a translationally invariant system their vertical excitations can be expressed as

$$|\Phi(K)\rangle = a^{TT}(K)\,|\Phi_m^{TT}(K)\rangle + a^{\text{e-h}}(K)\,|\Phi_n^{\text{e-h}}(K)\rangle\,, \tag{19}$$

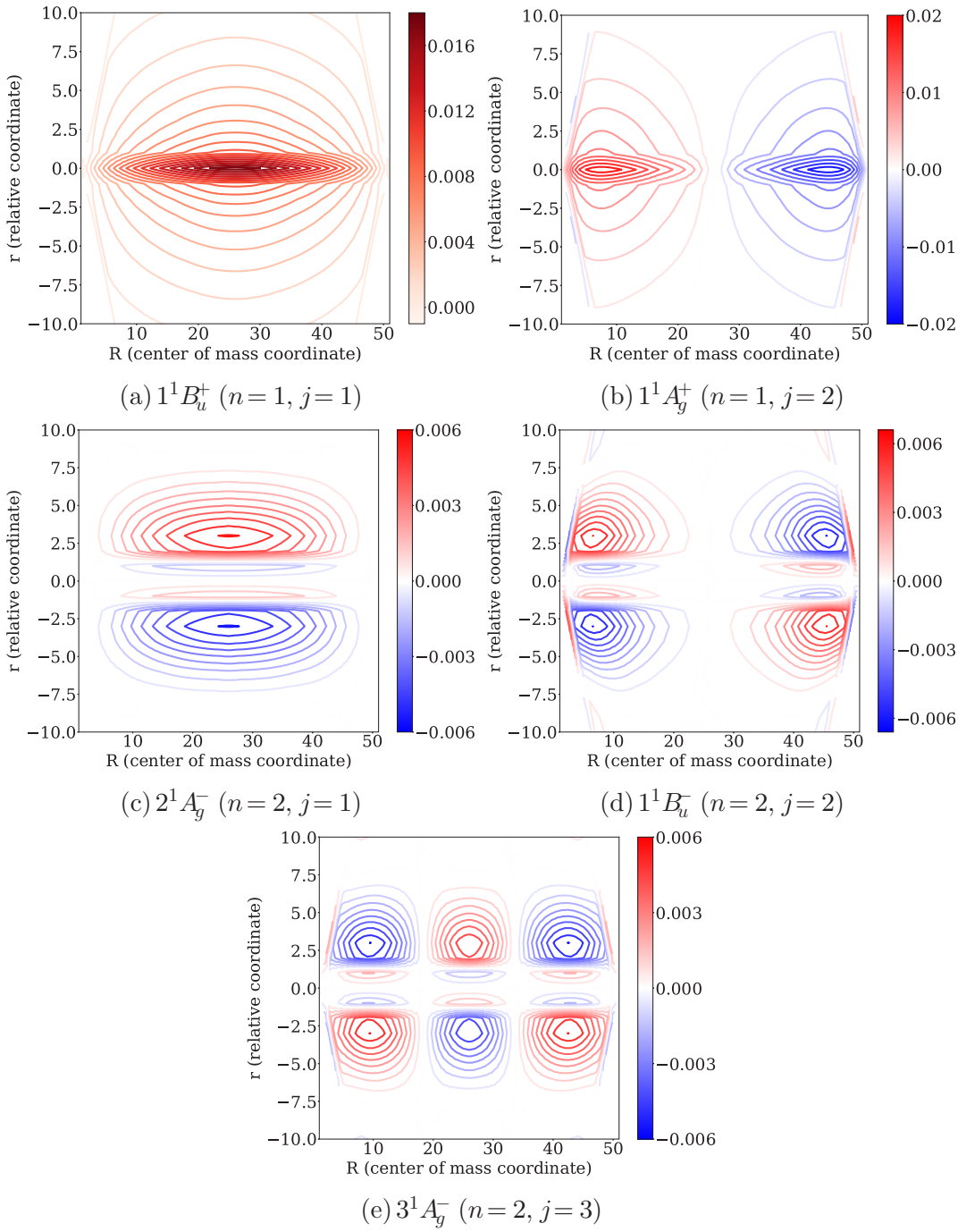

FIG. 8. Exciton components obtained from Eq. (18). n and j are the exciton principal and center-of-mass quantum numbers, respectively.

where $|\Phi_m^{TT}(K)\rangle$ is given by Eq. (13) and $|\Phi_m^{\text{e-h}}(K)\rangle$ is given by the Fourier transform of Eq. (17). Both components are labeled by the same center-of-mass quantum number K, but the principal quantum numbers for the triplet-pair (m) and electron-hole (n) components are different, being 1 and 2, respectively.

Equation (19) conveys the concept that the $2\,^1A_g^-$, $1\,^1B_u^-$, and $3\,^1A_g^-$ states are the three lowest-energy members of the same set of fundamental vertical excitations which are distinguishable only by their center-of-mass momentum [55].

VII. ABSORPTION SPECTRA

As the low-energy states have triplet-pair components, we might expect their absorption spectra to resemble that of the $1\,^3B_u^-$ and $1\,^3A_g^-$ triplet states. We calculated the approximate spectra of the $2\,^1A_g^-$, $3\,^1A_g^-$, $1\,^1B_u^-$, $1\,^5A_g^-$, $1\,^3B_u^-(T_1)$, and $1\,^3A_g^-(T_2)$ states for $N = 26$ using the expression

$$I(E) = \sum_i |\langle i \,|\, \hat{\mu} \,|\, \Psi\rangle|^2 \delta(E_i - E_\Psi - E), \qquad (20)$$

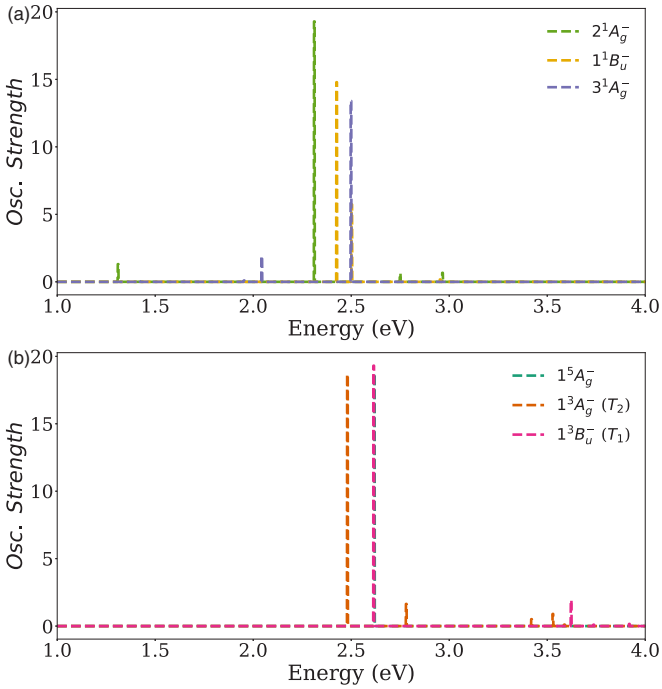

FIG. 9. Absorption spectra calculated using Eq. (20) of the (a) $2\,^1A_g^-$, $3\,^1A_g^-$, and $1\,^1B_u^-$ states and (b) $1\,^5A_g^-$, $1\,^3B_u^-(T_1)$, and $1^3A_g^-(T_2)$ for a 26-site chain.

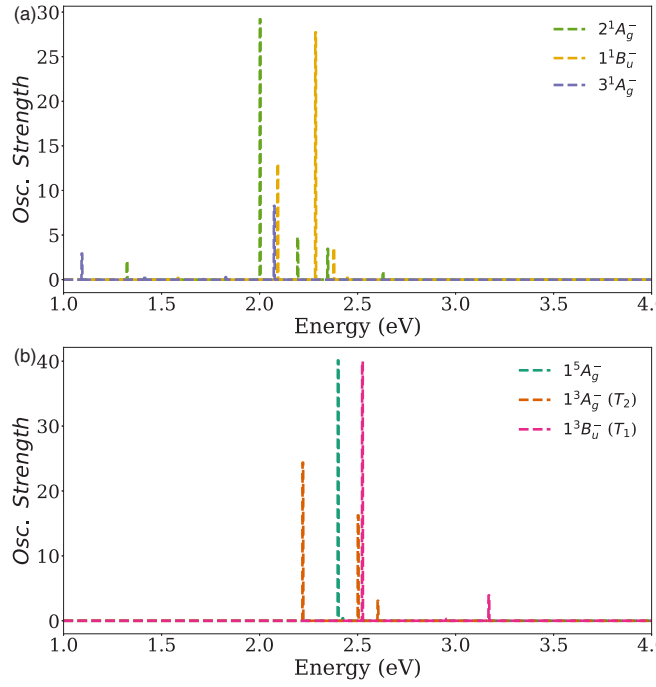

FIG. 10. Absorption spectra calculated using Eq. (20) of the (a) $2\,^1A_g^-$, $3\,^1A_g^-$, and $1\,^1B_u^-$ states and (b) $1\,^5A_g^-$, $1\,^3B_u^-(T_1)$, and $1\,^3A_g^-(T_2)$ for a 54-site chain.

where the sum is over states with opposite particle-hole and C_2 symmetry to the state $|\Psi\rangle$. $(E_i - E_\Psi)$ is the energy difference between state i and state Ψ, $\hat{\mu}$ is the transition dipole operator, and $|\langle i\,|\,\hat{\mu}\,|\,\Psi\rangle|^2$ is square of the transition dipole moment between states i and Ψ.

As shown in Figs. 9 and 10, for all of the triplet-pair states, the maximum absorption occurs within ∼0.5 eV of the $1\,^3B_u^-$ maximum absorption. Given that the $2\,^1A_g^-$ state is considered to be a bound triplet pair, we might expect that the maximum absorption energy to be higher than the triplet state, as a photoexcitation would need to overcome the binding energy of the triplet, in addition to having enough energy to excite a triplet state. However, the maximum absorption of the $2\,^1A_g^-$ state is found to be lower than the $1\,^3B_u^-$ state, in agreement with experimental observations in carotenoids [56]. The $2\,^1A_g^-$ state also has an absorption in the near infrared part of the spectrum, which can be attributed to the $2\,^1A_g^- \rightarrow 1\,^1B_u^+$ transition. The near infrared absorption of a bound triplet pair, which has also been predicted in acene materials by Khan and Mazumdar as a signature of electron-electron interactions [57], has been observed in a number of singlet fission materials [58–60].

The $1\,^5A_g^-$ quintet state exhibits a single absorption with energy closest to the triplet maximum absorption over all chain lengths and whose intensity most closely matches the $1\,^3B_u^-$ absorption. Comparing the $1\,^1B_u^-$ to the triplets, for each triplet absorption there is a corresponding redshifted absorption in the $1\,^1B_u^-$ spectra, also indicating that despite being a bound state, absorption are lower in energy compared to individual triplets.

Due to the mixed triplet-pair character of the $3\,^1A_g^-$ state there are many different absorptions. As for the $2\,^1A_g^-$ state, the $3\,^1A_g^-$ state has a lower energy absorption in the infrared to yellow portion of the spectrum.

We note that although our calculated transition energy from the $1\,^5A_g^-$ state coincides with our calculated T-T^* transition energy (i.e., ∼2.56 eV for the 26-site chain) this energy is over an eV higher than the observed T-T^* transition energy in conjugated polyenes [6,10]. We explain this discrepancy to the failure of the Mazumdar and Chandross parametrization of the PPP model to correctly estimate the solvation energy of weakly bound excitons and charges [33]. The T^* state is expected to be the $n = 2$ (charge-transfer) triplet exciton, whose solvation energy is over an eV larger than predicted by the parametrized PPP model [61].

VIII. DISCUSSION AND CONCLUSIONS

By calculating the relaxed energies of the singlet states of conjugated polyenes, we find that the $1\,^1B_u^-$ and $3\,^1A_g^-$ states lie below the bright $1\,^1B_u^+$ state at experimentally relevant chain lengths. This implies that these states could be involved in relaxation pathways, particularly if systems are excited with energy higher than the band edge. In addition, we find that the energy of the relaxed $1\,^5A_g^-$ state on a chain of N C atoms is twice the energy of the relaxed triplet state on a chain of $N/2$ C atoms, so if spin mixing were allowed this state could represent an intermediate unbound triplet-pair state for the singlet fission process.

An analysis of the bond dimerization of the relaxed excitations indicates that the $2\,^1A_g^-$ is a four-soliton state, as previously found [45]. The $1\,^5A_g^-$ and $1\,^1B_u^-$ states are also found to be four-soliton states. Both of these states seem to

consist of repelling soliton pairs, with the bond dimerization of the $1\,^5A_g^-$ resembling two $1\,^3B_u^-$ triplets occupying either side of the chain. The $3\,^1A_g^-$ state bond dimerization is more complicated due to the mixed triplet-pair combinations that contribute to this state.

The spin-spin correlation function offers another way to visualize the soliton structure. This again indicates that the $2\,^1A_g^-$ is a bound triplet pair. We also find that the $1\,^5A_g^-$ and $1\,^1B_u^-$ states show long-range spin correlations, which correspond to the staggered bond dimerization.

The calculated absorption spectra indicate that the $1\,^5A_g^-$ state most closely resembles the triplet absorption, although the $1\,^1B_u^-$ and $3\,^1A_g^-$ states also absorb at a similar energy. Recent pump-push-probe experiments by Pandya *et al.* excited the $2\,^1A_g^-$ state (push) after being generated from the relaxation of the initially photoexcited state [62]. As the $2\,^1A_g^-$ state has $^1(T_1T_1)$ character, the excited push state is expected to be of $^1(T_1T^*)$ character. Relaxation from this state was found to involve a state with spatially separated, but correlated triplet pairs. We predict that this state is either the $1\,^1B_u^-$ or $3\,^1A_g^-$ state [62].

We further analyzed the triplet-pair nature of the $2\,^1A_g^-$, $3\,^1A_g^-$, and $1\,^1B_u^-$ states by calculating the overlap of these states with half-chain triplet combinations. The $T_1 \otimes T_1$ nature of the $2\,^1A_g^-$ and $T_1 \otimes T_2$ nature of the $1\,^1B_u^-$ state was confirmed, while the $3\,^1A_g^-$ state has a mixture of $T_1 \otimes T_1$, and symmetry allowed $T_1 \otimes T_2$ and $T_2 \otimes T_2$ contributions. The higher-energy triplet-pair contributions to these singlet states was rationalized by a k-space analysis. We also showed that the electron-hole excitation components of the $2\,^1A_g^-$, $1\,^1B_u^-$, and $3\,^1A_g^-$ states belong to the same $n = 2$ family of excitons with center-of-mass quantum numbers $j = 1$, 2, and 3, respectively.

One of the aims of this work has been to identify a singlet state in polyenes that is intermediate between the initially photoexcited singlet state S_2 and the final nongeminate pair of triplet states. Such a state should satisfy the following conditions:

(1) It should have significant triplet-pair character.

(2) Its vertical energy should lie above the vertical energy of S_2, but its relaxed energy should lie below the relaxed energy of S_2. Such conditions imply the possibility of an efficient interconversion from S_2 via a conical intersection.

(3) Its relaxed energy should lie slightly higher than twice the relaxed energy of the triplet state, so that fission is potentially fast and exothermic.

For our choice of model parameters we find that: the $2\,^1A_g^-$ state only satisfies condition (1); the $1\,^1B_u^-$ state satisfies condition (1), conditions (2) for $10 < N < 26$, but not condition (3); the $3\,^1A_g^-$ state satisfies condition (1), conditions (2) for $20 < N < 46$, and condition (3) for all N. Thus, the $3\,^1A_g^-$ state would appear to be a candidate intermediate state for longer polyenes, but such a state does not exist for shorter carotenoids.

We should be cautious, however, about making a prediction about the precise intermediate state, as owing to using semiempirical parameters our calculated excitation energies are only expected to be accurate to within a few tenths of an eV. Our key conclusion, therefore, is that there is a family of singlet excitations (the $2\,^1A_g^-$ family), composed of both triplet-pair and electron-hole character, which are fundamentally the same excitation (i.e., have the same principal quantum numbers), but have different center-of-mass energies. The lowest energy member of this family, the $2\,^1A_g^-$ state, cannot undergo singlet fission. But higher-energy members, owing to their increased kinetic energy and reduced electron-lattice relaxation compared to two free triplets, can undergo singlet fission for certain chain lengths.

Based on energetic considerations, we are able to conclude that there are candidate triplet-pair states that might undergo singlet fission in polyenes only because our model contains both electron-electron and electron-nuclear interactions, and we are able to compute these energies for long chains. As Fig. 2 indicates, no vertically excited state satisfies both conditions (2) and (3).

A mechanism for singlet fission in molecular aggregates composed of short polyenes has been proposed by Aryanpour and co-workers [21]. This mechanism, involving interchain polaron pairs and intrachain excitons, is similar in spirit to the widely recognised mechanism for singlet fission in acene materials. This might be a competing mechanism in polyene aggregates to an intrachain process.

We are currently investigating the dynamics of interconversion to the $2\,^1A_g^-$ family from S_2 using time-dependent DMRG. It is tempting to assign the $3\,^1A_g^-$ state (or one of its relatives) as the geminate triplet pair, often denoted as $^1(T\cdots T)$. Noting that each component of a nongeminate triplet pair might reside on different chromophores on the same chain or on different chains, a possible mechanism to explain how $^1(T\cdots T)$ undergoes spin decoherence to become a nongeminate pair is described in the recent paper by Marcus and Barford [15].

ACKNOWLEDGMENTS

The authors thank Jenny Clark, Max Marcus, and Isabel V. L. Wilkinson for helpful discussions. D.V and D.M. would like to thank the EPSRC Centre for Doctoral Training, Theory and Modelling in Chemical Sciences, under Grant No. EP/L015722/1, for financial support. D.V. would also like to thank Balliol College Oxford for a Foley-Béjar Scholarship. D.M. would also like to thank Linacre College for a Carolyn and Franco Giantruco Scholarship and the Department of Chemistry, University of Oxford.

[1] W. Shockley and H. J. Queisser, J. Appl. Phys. **32**, 510 (1961).

[2] M. B. Smith and J. Michl, Annu. Rev. Phys. Chem. **64**, 361 (2013).

[3] G. Lanzani, S. Stagira, G. Cerullo, S. De Silvestri, D. Comoretto, I. Moggio, C. Cuniberti, G. F. Musso, and G. Dellepiane, Chem. Phys. Lett. **313**, 525 (1999).

[4] G. Lanzani, G. Cerullo, M. Zavelani-Rossi, S. De Silvestri, D. Comoretto, G. Musso, and G. Dellepiane, Phys. Rev. Lett. **87**, 187402 (2001).

[5] M. R. Antognazza, L. Lüer, D. Polli, R. L. Christensen, R. R. Schrock, G. Lanzani, and G. Cerullo, Chem. Phys. **373**, 115 (2010).

[6] A. J. Musser, M. Al-Hashimi, M. Maiuri, D. Brida, M. Heeney, G. Cerullo, R. H. Friend, and J. Clark, J. Am. Chem. Soc. **135**, 12747 (2013).

[7] Y. Kasai, Y. Tamai, H. Ohkita, H. Benten, and S. Ito, J. Am. Chem. Soc. **137**, 15980 (2015).

[8] E. Busby, J. Xia, Q. Wu, J. Z. Low, R. Song, J. R. Miller, X. Y. Zhu, L. M. Campos, and M. Y. Sfeir, Nat. Mater. **14**, 426 (2015).

[9] B. Kraabel, D. Hulin, C. Aslangul, C. Lapersonne-Meyer, and M. Schott, Chem. Phys. **227**, 83 (1998).

[10] A. J. Musser, M. Al-Hashimi, M. Heeney, and J. Clark, J. Chem. Phys. **151**, 044902 (2019).

[11] U. N. Huynh, T. P. Basel, E. Ehrenfreund, and Z. V. Vardeny, J. Phys. Chem. Lett. **9**, 4544 (2018).

[12] U. N. V. Huynh, T. P. Basel, E. Ehrenfreund, G. Li, Y. Yang, S. Mazumdar, and Z. V. Vardeny, Phys. Rev. Lett. **119**, 017401 (2017).

[13] J. Hu, K. Xu, L. Shen, Q. Wu, G. He, J. Y. Wang, J. Pei, J. Xia, and M. Y. Sfeir, Nat. Commun. **9**, 1 (2018).

[14] A. Rao and R. H. Friend, Nat. Rev. Mater. **2**, 17063 (2017).

[15] M. Marcus and W. Barford, Phys. Rev. B **102**, 035134 (2020).

[16] R. J. Bursill and W. Barford, Phys. Rev. Lett. **82**, 1514 (1999).

[17] W. Barford, *Electronic and Optical Properties of Conjugated Polymers* (Oxford University Press, Oxford, 2013).

[18] W. Barford, R. J. Bursill, and M. Y. Lavrentiev, Phys. Rev. B. **63**, 195108 (2001).

[19] J. Ren, Q. Peng, X. Zhang, Y. Yi, and Z. Shuai, J. Phys. Chem. Lett. **8**, 2175 (2017).

[20] K. Aryanpour, T. Dutta, U. N. V. Huynh, Z. V. Vardeny, and S. Mazumdar, Phys. Rev. Lett. **115**, 267401 (2015).

[21] K. Aryanpour, A. Shukla, and S. Mazumdar, J. Phys. Chem. C **119**, 6966 (2015).

[22] M. Schmidt and P. Tavan, J. Chem. Phys. **136**, 124309 (2012).

[23] P. Tavan and K. Schulten, Phys. Rev. B **36**, 4337 (1987).

[24] W. Hu and G. K.-L. Chan, J. Chem. Theory Comput. **11**, 3000 (2015).

[25] C. Wang, D. E. Schlamadinger, V. Desai, and M. J. Tauber, Chem. Phys. Chem. **12**, 2891 (2011).

[26] J. Yu, L. M. Fu, L. J. Yu, Y. Shi, P. Wang, Z. Y. Wang-Otomo, and J. P. Zhang, J. Am. Chem. Soc. **139**, 15984 (2017).

[27] E. J. Taffet, B. G. Lee, Z. S. D. Toa, N. Pace, G. Rumbles, J. Southall, R. J. Cogdell, and G. D. Scholes, J. Phys. Chem. B **123**, 8628 (2019).

[28] H. Hashimoto, C. Uragami, N. Yukihira, A. T. Gardiner, and R. J. Cogdell, J. R. Soc. Interface **15**, 20180026 (2018).

[29] M. J. Tayebjee, S. N. Sanders, E. Kumarasamy, L. M. Campos, M. Y. Sfeir, and D. R. McCamey, Nat. Phys. **13**, 182 (2017).

[30] L. R. Weiss, S. L. Bayliss, F. Kraffert, K. J. Thorley, J. E. Anthony, R. Bittl, R. H. Friend, A. Rao, N. C. Greenham, and J. Behrends, Nat. Phys. **13**, 176 (2017).

[31] S. N. Sanders, A. B. Pun, K. R. Parenti, E. Kumarasamy, L. M. Yablon, M. Y. Sfeir, and L. M. Campos, Chem **5**, 1988 (2019).

[32] R. E. Merrifield, Pure Appl. Chem. **27**, 481 (1971).

[33] M. Chandross and S. Mazumdar, Phys. Rev. B **55**, 1497 (1997).

[34] U. Schollwöck, Rev. Mod. Phys. **77**, 259 (2005).

[35] S. R. White, Phys. Rev. Lett. **69**, 2863 (1992).

[36] W. Barford, R. J. Bursill, and M. Y. Lavrentiev, Phys. Rev. B **65**, 075107 (2002).

[37] R. J. Bursill and W. Barford, Phys. Rev. B **66**, 205112 (2002).

[38] R. J. Bursill and W. Barford, J. Chem. Phys. **130**, 234302 (2009).

[39] Y. Kurashige, H. Nakano, Y. Nakao, and K. Hirao, Chem. Phys. Lett. **400**, 425 (2004).

[40] This observation of the triplet-pair character of the quintet state is often invoked for simpler models, but remains valid with interacting electrons and electron-nuclear coupling [10].

[41] M. W. Wilson, A. Rao, K. Johnson, S. Gélinas, R. Di Pietro, J. Clark, and R. H. Friend, J. Am. Chem. Soc. **135**, 16680 (2013).

[42] C. E. Swenberg and W. T. Stacy, Chem. Phys. Lett. **2**, 327 (1968).

[43] O. R. Tozer and W. Barford, Phys. Rev. B **89**, 155434 (2014).

[44] A. J. Heeger, S. Kivelson, J. R. Schrieffer, and W. P. Su, Rev. Mod. Phys. **60**, 781 (1988).

[45] G. W. Hayden and E. J. Mele, Phys. Rev. B **34**, 5484 (1986).

[46] S. Roth and D. Carroll, *One-dimensional metals : conjugated polymers, organic crystals, carbon nanotubes and graphene* (Wiley, New York, 2015), p. 1.

[47] W. P. Su, Phys. Rev. Lett. **74**, 1167 (1995).

[48] Or more correctly, spinon character.

[49] In this paper we adopt the chemists' definition of particle-hole symmetry, which is opposite to the physicists' notation (see Ref. [17]). The chemists' notation coincides with the electron-hole parity of excited states, described in Sec. VI C.

[50] A. B. Harris, Phys. Rev. B **7**, 3166 (1973).

[51] G. S. Uhrig and H. J. Schulz, Phys. Rev. B **54**, R9624(R) (1996).

[52] W. Barford, R. J. Bursill, and R. W. Smith, Phys. Rev. B **66**, 115205 (2002).

[53] W. Barford, J. Phys. Chem. A **117**, 2665 (2013).

[54] W. Barford and N. Paiboonvorachat, J. Chem. Phys. **129**, 164716 (2008).

[55] A band of triplet states was predicted in the early work of Ref. [23]. In a linear chain with four carbons, T_1 (i.e., $1\,^3B_u$) and T_2 (i.e., $1\,^3A_g$) are the superpositions $[(C_1-C_2)_S(C_3-C_4)_T \pm (C_1-C_2)_T(C_3-C_4)_S]$ where the suffixes refer to singlet (S) and triplet (T) bonds. The plus and minus combinations correspond to the $k=0$ and π superpositions. In longer open chains there will be superpositions that correspond to intermediate $0<k<\pi$ states, i.e., to a band of triplets (see also Refs. [50,51] for a discussion of the triplet spectrum in Heisenberg antiferromagnetic chains).

[56] D. W. Polak, A. J. Musser, G. A. Sutherland, A. Auty, F. Branchi, B. Dzurnak, J. Chidgey, G. Cerullo, C. N. Hunter, and J. Clark, arXiv:1901.04900.

[57] S. Khan and S. Mazumdar, J. Phys. Chem. C (2020).

[58] M. T. Trinh, A. Pinkard, A. B. Pun, S. N. Sanders, E. Kumarasamy, M. Y. Sfeir, L. M. Campos, X. Roy, and Y. Zhu, Sci. Adv. **3**, e1700241 (2017).

[59] K. Miyata, F. S. Conrad-Burton, F. L. Geyer, and X. Y. Zhu, Chem. Rev. **119**, 4261 (2019).

[60] A. N. Stuart, P. C. Tapping, E. Schrefl, D. M. Huang, and T. W. Kee, J. Phys. Chem. C **123**, 5813 (2019).

[61] W. Barford, N. Paiboonvorachat, and D. Yaron, J. Chem. Phys. **134**, 234101 (2011).

[62] R. Pandya, Q. Gu, A. Cheminal, R. Y. S. Chen, E. P. Booker, R. Soucek, M. Schott, L. Legrand, F. Mathevet, N. C. Greenham, T. Barisien, A. J. Musser, A. W. Chin, and A. Rao, arXiv:2002.12465.